10TH INTERNATIONAL SYMPOSIUM ON PARTICLE IMAGE VELOCIMETRY - PIV13
Delft, The Netherlands, July 1-3, 2013

Astigmatism Particle Tracking Velocimetry for Macroscopic Flows

Thomas Fuchs, Rainer Hain and Christian J. Kähler

Bundeswehr University Munich, Institute of Fluid Mechanics and Aerodynamics
Werner-Heisenberg-Weg 39, 85577 Neubiberg, thomas.fuchs@unibw.de

Abstract

Astigmatism Particle Tracking Velocimetry (APTV) is a three-dimensional flow measurement technique. It requires only a single camera and is therefore best suited for measurement domains with limited optical access, such as compressor and combustion research. The z-component of the spatial particle position is coded in the geometry of its particle image. In order to prove the feasibility of APTV to measure macroscopic air flows, an accuracy analysis using a pinhole matrix (pinhole diameter of 1.1 ± 0.1 μm) is carried out. Two different optical setups with different measurement depths (20-100 mm) are investigated. The relative measurement error lies in the range of 0.34-0.46 % of the measurement depth. Altogether APTV allows for accurate volumetric velocity measurements in macroscopic air flows.

1. Introduction

The simultaneous measurement of all three velocity components in a volume is of great interest in many fluid mechanical applications. Therefore several measurement techniques, based on Particle Image Velocimetry (PIV) and Particle Tracking Velocimetry (PTV), have been developed [1]. In microfluidics a well-established 3D3C measurement technique is the so-called Astigmatism-PTV (APTV) [2, 3]. This technique requires only a single camera and is thus best suited for applications with limited optical access compared to multi-camera techniques like TOMO-PIV [4]. APTV takes advantage of an optical aberration, namely astigmatism, induced by a cylindrical lens, leading to the appearance of a sagittal and a meridional focal plane. Due to this aberration, a seeding particle forms an elliptical particle image with a distinct geometry corresponding to the distance from the camera. Hence, the z-position along the optical axis of a particle is coded in the axis lengths of the elliptical particle image, whereas its x- and y-position is determined by the particle image's center. With the knowledge of the spatial positions of the particles, the velocity field is calculated by means of a tracking algorithm. The depth encoding scheme is illustrated in Fig. 1.

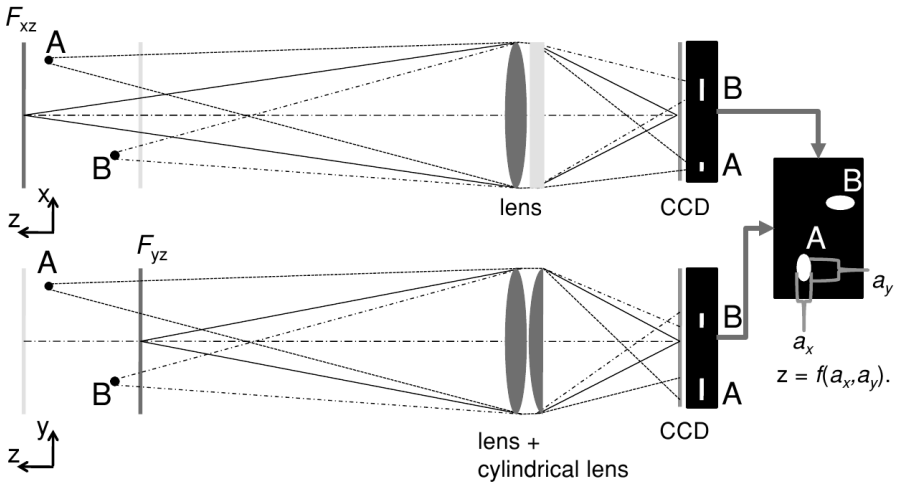

Figure 1: Principle setup of the optical components. In the xz-plane only the spherical lens acts, whereas in the yz-plane both lenses are acting [5]

In order to prove the practicability of APTV in macroscopic domains, an accuracy analysis of the particle position determination is carried out. The analysis focuses on the z-coordinate of the location, as this coordinate, along the optical axis, is the one with the lowest accuracy. The following section outlines the experimental method of the accuracy analysis followed by an analysis and discussion of the results.

2. Experimental Setup and Method

For the accuracy analysis a backlight illuminated pinhole matrix (pinhole diameter: 1.1±0.1 μm, vertical and horizontal displacement of the pinholes: 4 mm) is moved through the entire measurement depth in steps of Δz (note that the light emission behaviour of particles and pinholes is similar). At each location 20 images are recorded. Two setups with different cylindrical lenses are investigated, one with a focal length of $f_{zylA} = 500$ mm (setup A) and one with $f_{zylB} = 1000$ mm (setup B). While the working distance (280 mm) is equal for both setups, the employment of different cylindrical lenses leads to different distances of the focal planes and thus measurement volumes. For setup A the focal plane distance is $\Delta z_{FPA} \approx 52$ mm (Δz_{FPB} is about 22.5 mm). The images are recorded with a *LaVision sCMOS* camera with an objective lens of 50 mm focal length and a f-number of 8 (setup A) and 11 (setup B).

Due to the properties of the pinhole matrix (a photo mask with a very thin chromium layer with a total of 400 etched pinholes over an area of 80×80 mm^2), it is not possible to illuminate the pinhole matrix at an angle of 0 degree to the optical axis. The chromium layer does not fully block the light. For this reason the laser light (2.5 W cw-laser at a wave length of 532 nm) directly illuminates the camera sensor, which is then overexposed. This makes an illumination at an angle greater than 0 degree to the optical axis necessary. On the other hand the larger the angle of illumination is, the lower the emitted light intensity of a pinhole is, if the angular intensity distribution of light diffraction on a circular aperture is considered [6]. With an illumination angle of approximately 10 degree to the optical axis, a setup is found where a reasonable high light emission from the pinholes is provided, while at the same time the camera is in a save position. However, as a consequence the illuminated area of the pinhole matrix fills roughly half the sensor size (for setup A 852×983 pixel of 2560×2160 pixel, see the grey box in Fig. 3, setup B: 759×1000). Another point is that the light that is not absorbed by the chromium layer also illuminates the objective lens placed in front of the pinhole matrix. This in turn causes reflections affecting the camera sensor as the chromium layer has mirroring properties. Hence, the field of view (FOV) is reduced further and the signal-to-noise ratio (SNR) of the pinhole images is decreasing. The resulting FOV for setup A is 13.1×15.1 mm^2 at $z = 0$ mm changing linearly to 21.8×25.2 mm^2 at $z = 100$ mm. For setup B the FOV is 13.3×17.5 mm^2 at $z = 0$ mm and 17.2×22.6 mm^2 at $z = 50$ mm.

The geometry of a pinhole image does not only depend on the distance to the camera but also on its X- and Y-position, as the focal planes are curved. In addition, distortions in the optical path (such as windows, lens imperfections etc.) have to be accounted for. Thus, it is necessary to establish a calibration function depending on the geometry of a pinhole image and the X-, Y- and z-coordinates of the corresponding pinhole. The first step of the calibration procedure is to calculate an intensity averaged image of the 20 images recorded at each z-position. This is followed by a spline fit of the axis ratio values of the averaged pinhole images at each location. Then the X- and Y-position of a pinhole image is determined, leading to a calibration function depending on the z-coordinate for this specific pinhole image (the axis ratio values are derived from the spline fits at every z-position). Fig. 2 illustrates the described principle.

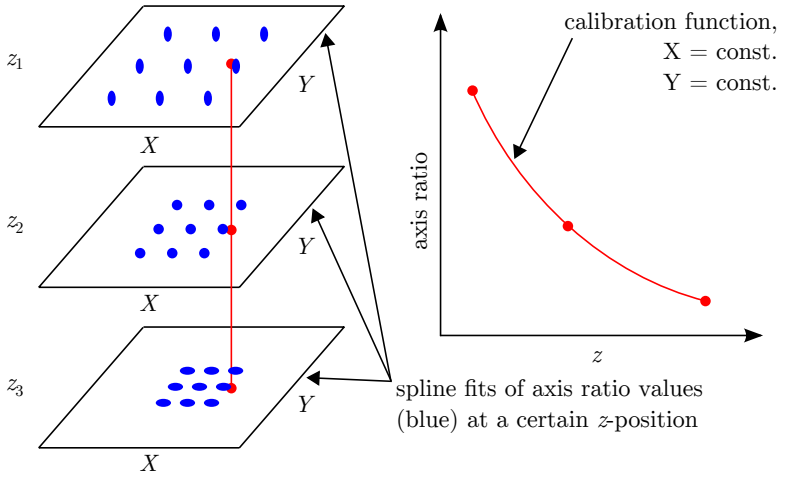

Figure 2: Calibration scheme: At first axis ratio values are fitted (spline fit) at every z-position. After that a calibration curve for the X- and Y-position of a pinhole image is established, where the depth position is determined by the axis ratio of the pinhole image (red curve).

For specific X- and Y-positions the calibration functions are given in Fig. 3 (setup A). Each the maximum and the minimum value of the axis ratios denote a focal plane. The functions are not exactly point-symmetric as with distance to the pinhole matrix the signal-to-noise ratio is decreasing, resulting in less accentuated diffraction images.

Following this calibration procedure the absolute deviation, ΔZ, of the calculated pinhole position compared to the actual position is determined at every z-position (see Fig. 4). This leads to a database of 20 pinhole images in each of the 20 recordings at every z-position (i.e. 400 pinhole images per z-position). However, it can be seen that the calibration function is ambiguous when measuring beyond the focal planes. These ambiguities can be overcome in the following way. Whereas the axis ratio has a minimum or a maximum at the focal planes, the larger axis of a particle image changes lineary near the corresponding focal plane. Thus, the length of the larger axis determines whether the particle position is within or beyond a focal plane. In the next section the results of the accuracy studies, performed as outlined here, are analyzed for setups A and B.

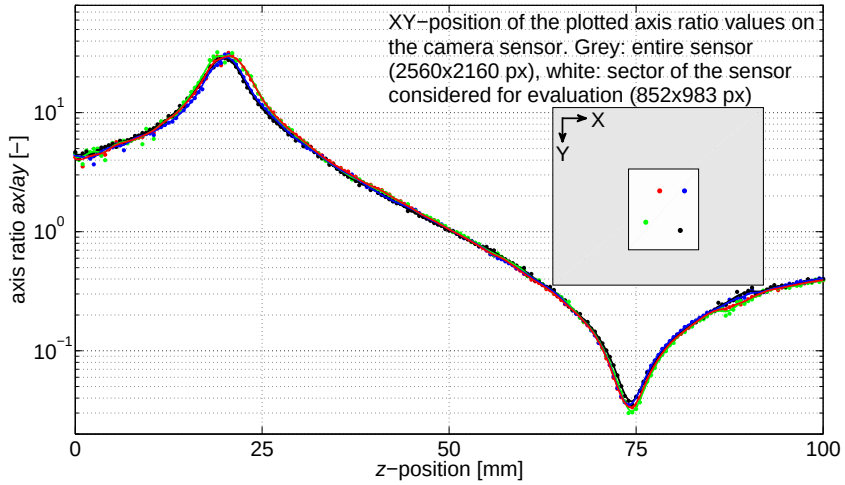

Figure 3: Calibration functions at different x- and y-positions are shown for setup A. The axis ratios are derived from the spline fits at every z-position. The images are recorded with a step width of $\Delta z_A = 0.5$ mm (setup A) along z. Setup B has a step width of $\Delta z_B = 0.25$ mm (not shown here).

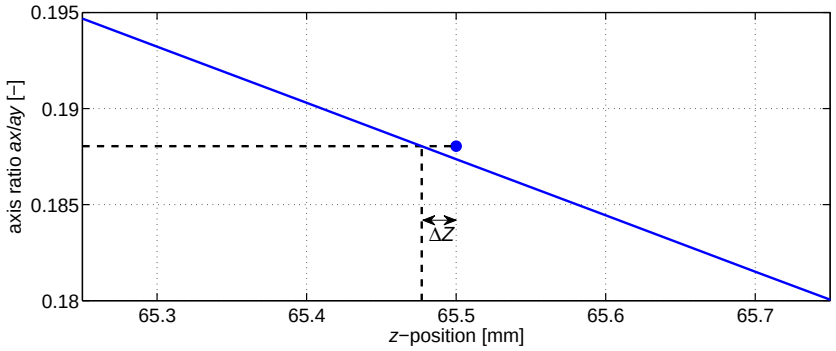

Figure 4: z-position determination scheme: The deviation of the real depth position of a pinhole to the measured one is denoted by ΔZ. From this deviation the measurement error is determined.

3. Results and Analysis

In the following the results of the accuracy analysis, conducted as described in the preceding paragraph, are analyzed. For setup A an average measurement error of 0.17 mm is found between the focal planes. It is about 0.34 % of the measurement depth of 50 mm (see Fig. 5a). When going beyond the focal planes the average error increases to 0.41 mm (or 0.41 %) at a measurement depth of 100 mm (see Fig. 5b). Note that also the error between the focal planes increases, despite the fact that the data set is the same. This is due to an adjustment of the processing algorithm in order to be able to process the larger (therefore lower SNR) pinhole images beyond the focal planes. Fig. 5b shows the largest measurement error to be in the area beyond the focal planes, where pinhole images with low SNRs are found. At both focal planes the measurement error has peaks even though the SNRs are the largest. This can be explained by the calibration function which has a maximum or minimum at the respective focal planes. Generally, the measurement error increases with a decreasing slope of the calibration function.

The measurement errors of setup B are significantly smaller. Between the focal planes an error of 0.07 mm occurs, being equivalent to 0.35 % of the measurement depth of 20 mm (see Fig. 5c). The measurement error of the entire measurement depth is 0.23 mm, i.e. 0.46 % of 50 mm (see Fig. 5d). However, it would be expected that the error of setup B is higher as the amount of astigmatism is lower (focal length of cylindrical lens is 1000 mm compared to 500 mm for setup A) and therefore smaller absolute axis lengths of the pinhole images occur. But in turn the light intensity emitted by a pinhole is distributed over a larger area on the sensor, leading to a lower SNR. Hence, a low SNR has a strong negative impact on the accuracy of the spatial pinhole position determination. Altogether the measurement error with respect to the measurement depth (0.34-0.46 %) is in a similar range.

Preliminary accuracy investigations conducted with a single pinhole of 5 μm diameter show lower measurement errors. The depth position can be determined with an accuracy of 0.07 mm over a measurement depth of 120 mm. While the shape and size of a pinhole

image does not differ significantly between a 1 μm and a 5 μm diameter pinhole, the main reason for the higher accuracy of the larger pinhole is the higher SNR. Furthermore, the spline fit of the axis ratio values of the pinhole matrix at every z-position yields an additional error. If single pinholes of the matrix are analyzed separately (i.e. each pinhole has its own calibration function) the measurement error decreases to 0.1 mm compared to 0.17 mm for setup A. In this case the error of setup B is 0.05 mm (before: 0.07 mm).

With the lower SNR of the 1 μm pinholes compared to the 5 μm pinholes minor changes in the diffraction patterns of the pinhole images are observed. The 5 μm pinhole image shows an asteroid shaped diffraction pattern (see [7] for further information) of a low intensity at both focal planes, which is observed for the 1 μm pinholes. This leads to different calibration functions near the focal planes as the brighter asteroid shaped diffraction pattern results in smaller maxima and larger minima of the axis ratio values. Hence, the calibration function in near focal regions is mainly determined by the SNR of the particle image. Between the focal planes, for both pinhole sizes, the calibration function is overlapping over a range of more than 90 % of the focal plane distance, Δz_{FP}, independent of the SNR.

APTV allows for high measurement accuracies in macroscopic flows compared to other similar techniques. For example, a technique employing an axicon for depth determination has a relative measurement error being more than 10 to 36 times higher [8], depending on the setup.

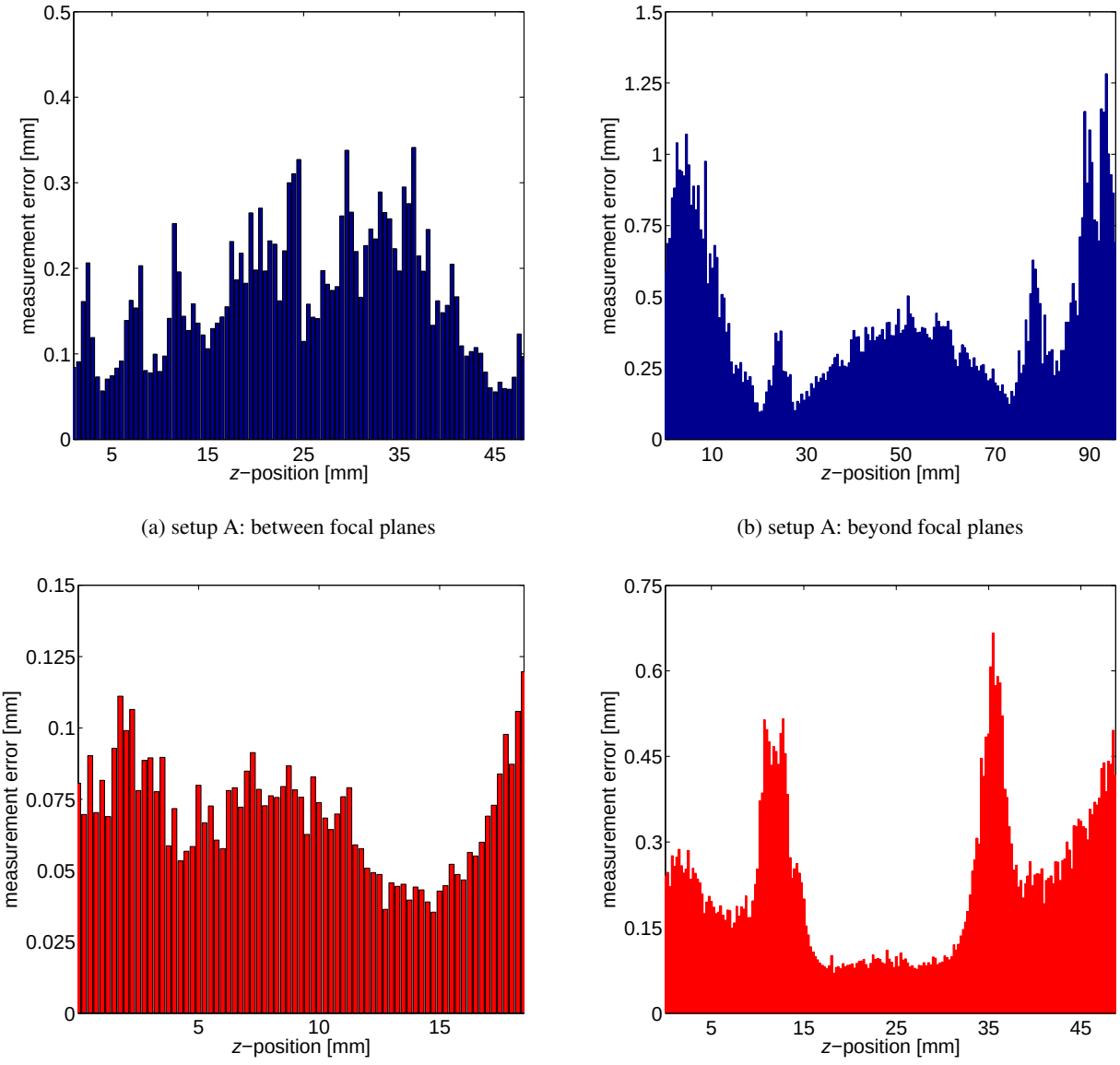

(a) setup A: between focal planes

(b) setup A: beyond focal planes

(c) setup B: between focal planes

(d) setup B: beyond focal planes

Figure 5: Measurement errors depending on the z-position for setups A and B. For setup A the average measurement error is 0.17 mm between the focal planes and 0.41 mm for the entire measurement depth. Setup B has a measurement error of 0.07 mm between the focal planes and 0.23 mm for the entire measurement depth.

4. Conclusion and Outlook

So far APTV has not been applied to macroscopic air flows. This study gives a realistic measure of the achievable depth position determination accuracy of particles with $d_p \approx 1$ μm. Furthermore, the outlined calibration procedure is well-suited for the proposed applications of APTV, namely in measurement environments with limited optical access, such as combustion and compressor flows. Windows and other optical influences are accounted for and therefore a true three-dimensional calibration procedure is enabled. Nonetheless, the calibration target (i.e. the pinhole matrix) has to be improved further. A smaller lateral displacement of the pinholes would improve the measurement error as with more supporting points the spline fit at every z-position is more accurate. Increasing the pinhole diameter to gain a larger SNR for the calibration images is also helpful. Additionally, the two-step calibration procedure could be replaced by a system of equations containing all the information required.

An interesting opportunity for APTV is the employment of a second camera with a slightly different viewing angle (still one optical access), where the depth position of a particle is calculated by means of triangulation. Therefore, a comparative study of TOMO-PIV and APTV is under way in order to analyze the capabilities of both measurement techniques in macroscopic flows.

Acknowledgement

The investigations were conducted as part of the joint research programme AG Turbo 2020 in the frame of AG Turbo. The work was supported by the Bundesministerium für Wirtschaft und Technologie (BMWi) as per resolution of the German Federal Parliament under grant number 03ET2013M. The authors gratefully acknowledge AG Turbo and MTU Aero Engines AG for their support and permission to publish this paper. The responsibility for the content lies solely with its authors.

REFERENCES

[1] Cierpka C and Kähler CJ "Particle imaging techniques for volumetric three-component (3D3C) velocity measurements in microfluidics" Journal of Visualization 15 (2012) pp.1-31

[2] Cierpka C et al. "A simple single camera 3C3D velocity measurement technique without errors due to depth of correlation and spatial averaging for microfluidics" Measurement Science and Technology 21 (2010) 045401

[3] Kao HP and Verkman AS "Tracking of Single Fluorescent Particles in Three Dimensions: Use of Cylindrical Optics to Encode Particle Position" Biophysical Journal 67 (1994) pp.1291-1300

[4] Scarano F "Tomographic PIV: principles and practice" Measurement Science and Technology 24 (2013) 012001

[5] Cierpka C et al. "On the calibration of astigmatism particle tracking velocimetry for microflows" Measurement Science and Technology 22 (2011) 015401

[6] Born M and Wolf E "Principles of Optics" 6^{th} Ed. (Pergamon Press, 1980) p.417

[7] Nienhuis K and Nijboer BRA "The diffraction theory of optical aberrations" Physica 14 (1949) pp.590-608

[8] Snoeyink C and Wereley S "Three-dimensional locating of paraxial point source with axicon" Optics Letters 37 (2012) pp.2058-2060